Monte Carlo simulation study of droplet nucleation

Alexander V. Neimark[a] and Aleksey Vishnyakov
Center for Modeling and Characterization of Nanoporous Materials, TRI/Princeton, Princeton, New Jersey 08542

(Received 28 June 2004; accepted 16 February 2005; published online 4 May 2005)

A new rigorous Monte Carlo simulation approach is employed to study nucleation barriers for droplets in Lennard-Jones fluid. Using the gauge cell method we generate the excess isotherm of critical clusters in the size range from two to six molecular diameters. The ghost field method is employed to compute the cluster free energy and the nucleation barrier with desired precision of $(1-2)kT$. Based on quantitative results obtained by Monte Carlo simulations, we access the limits of applicability of the capillarity approximation of the classical nucleation theory and the Tolman equation. We show that the capillarity approximation corrected for vapor nonideality and liquid compressibility provides a reasonable assessment for the size of critical clusters in Lennard-Jones fluid; however, its accuracy is not sufficient to predict the nucleation barriers for making practical estimates of the rate of nucleation. The established dependence of the droplet surface tension on the droplet size cannot be approximated by the Tolman equation for small droplets of radius less than four molecular diameters. We confirm the conclusion of ten Wolde and Frenkel [J. Chem. Phys. **109**, 9901 (1998)] that integration of the normal component of the Irving–Kirkwood pressure tensor severely underestimates the nucleation barriers for small clusters. © *2005 American Institute of Physics*. [DOI: 10.1063/1.1888389]

I. INTRODUCTION

Nucleation of droplets in a metastable vapor has been a case study problem in molecular simulations of phase transformations starting with the pioneering applications of Monte Carlo (MC) and molecular dynamics (MD) techniques by Lee, Barker, and Abraham,[1] McGinty,[2] and Rusanov and Brodskaya[3] in 1970s. In addition to recently revealed controversies of the simulation methods employed, which are discussed below, the interpretation of simulation results in terms of the Gibbs classical capillarity approximation[4–7] by introducing the droplet surface tension, and its dependence on the droplet size through the Tolman length is also ambiguous.

Nucleation is a complex nonequilibrium process. Direct MD simulations of nucleation are informative, but still limited to high supersaturations and, respectively, small nuclei.[8] Most simulation studies consider equilibrium systems and focus on the critical nucleus size and its free energy of formation. Even then, the problem of nucleation cannot be considered within the rigorous framework of statistical mechanics because the critical nucleus is entirely unstable in an open system. Indeed, any fluctuations of the critical nucleus would lead to either its decay or growth. In order to simulate critical nuclei, it is necessary to impose certain constraints on density fluctuations in the system, and then to account for these constraints in calculations of the system free energy. The most straightforward approach to impose such constraints is to consider a closed system with a fixed number of molecules, namely, a droplet confined to a finite volume cell in the canonical ensemble that was done by Lee, Barker, and Abraham (LBA).[1] The authors performed MC simulations of small Lennard-Jones (LJ) droplets (up to 100 molecules). In order to find the Helmholtz free energy of the droplet, a series of simulations were performed, in which the size of the confining cell was gradually increased, keeping the number of molecules fixed, until the vapor state was reached. The Helmholtz free energy was found from the volume dependence of the pressure, assuming that the pdV integral along this pass gives the reversible work of droplet formation. The pressure was determined by the virial equation. Although this approach was employed later many times, a validity of the virial equation for a heterogeneous system confined to a small volume has been recently questioned by Reiss and Reguera.[9] Another shortcoming of the LBA approach is an assumption that a droplet in a finite system can be formed (evaporated) by increasing (decreasing) the system volume reversibly at a constant loading. Indeed, as was shown by Binder[10] for the Ising model and discussed recently in details by Reguera *et al.*[11] for the LJ fluid, the vapor-to-droplet transition in a finite system necessarily contains a spontaneous step that makes impossible constructing a continuous trajectory of equilibrium states for thermodynamic integration. A comprehensive analysis of this phenomenon is given elsewhere.[12]

Another approach to determining the Helmholtz free energy of a droplet generated in the canonical ensemble was introduced by Rusanov and Brodskaya[3] (RB) in 1977. The authors calculated the normal component of the Irving–Kirkwood pressure tensor of small LJ droplets of various sizes (up to 500 molecules) in a series of MD simulations. Integrating the normal component of the pressure tensor, they found the location of the surface of tension of the ref-

[a]Author to whom correspondence should be addressed. Electronic mail: aneimark@triprinceton.org

erence spherical droplet and the droplet surface tension γ, and respectively, the work of droplet formation according to the capillarity approximation through the Gibbs formula,[6]

$$\Delta\Omega_d = \frac{4\pi}{3} r_s^2 \gamma_s = \frac{2\pi}{3}(\Delta p) r_s^3 = \frac{16\pi\gamma_s^3}{3(\Delta p)^2}, \tag{1}$$

where γ_s is the surface tension referred to the surface of tension of radius r_s, which fulfills the Laplace equation (2) for the pressure difference, $\Delta p = p_l - p_v$, between the liquid and vapor phases labeled by subscripts "l" and "v,"

$$\Delta p = \frac{2\gamma_s}{r_s}. \tag{2}$$

The vapor pressure p_v was evaluated from the averaging of the pressure profile on the periphery of the simulation cell. p_l, the pressure in a bulk liquid at the chemical potential of the fluid in the droplet, was calculated from second virial coefficient. The surface tension was found to increase monotonically with the radius that implies positive δ. The authors fitted the dependence $\gamma_s(r_s)$ by the Tolman equation[7]

$$\gamma = \gamma_\infty \left(1 - \frac{2\delta}{r_s}\right), \tag{3}$$

where γ_∞ is the surface tension of plane surface and δ is the Tolman length independent of the droplet sizes. They obtained γ_∞ higher than the experimental value for argon and δ equal to 1.7σ (σ is the LJ molecular diameter).

RB (Ref. 3) recognized that the pressure tensor is not uniquely defined for a cluster as was noted by Harasima[13] back in 1956. Moreover, Shofield and Henderson[14] argued that it is not certain where a force between two molecules is acting, besides the molecules themselves. Whether the integral characteristics of a system are affected by the choice of the pressure tensor is still a matter of opinion controversy, especially when the system size is comparable with the range of intermolecular forces.[15] Despite of the lack of a rigorous foundation, the pressure tensor method has since been widely employed.[16–25]

Thomson *et al.*[16] performed MC and MD simulations of larger (maximum of 2048 particles) critical droplets and used the RB (Ref. 3) technique to obtain the surface tension and the location of the surface of tension. Their results were in qualitative agreement with those of Ref. 3. For larger droplets, the surface tension was close to the bulk value. The Tolman length δ was estimated as the difference between the equimolar radius r_c and the radius of tension r_s,

$$\delta = r_e - r_s. \tag{4}$$

The authors also applied a different "thermodynamic" method to obtain the surface tension and δ, assuming that the Tolman equation (3) with constant δ independent of cluster diameters was valid for droplets of all sizes from smallest clusters to plane interface. For almost all clusters they obtained positive values of δ ranging from zero to 1σ.

Extensive studies of the Tolman length were made by Nijmeijer *et al.*[17] who simulated large (up to 12 000 molecules) LJ clusters. The authors derived an expression for the surface tension, the radius of tension, and the Tolman length from the normal and tangential components of the pressure tensor, which is independent of the exact form of the tensor provided it complies with the microscopic condition of mechanical equilibrium $\nabla \mathbf{p} = 0$. They obtained small negative values of the Tolman length with a large statistical error due to significant statistical errors in the tangential component. In a subsequent discussion,[18,23] Brodskaya and Rusanov[23] re-evaluated the data of Nijmeijer[17] and obtained positive values of the Tolman length. Later, Haye and Bruin[19] obtained a positive value of the Tolman length for a similar cluster at a higher temperature.

ten Wolde and Frenkel[21] questioned the very validity of the pressure tensor calculations for small droplets. They demonstrated a striking disagreement with the results of the constant-pressure MC simulation of LJ droplets. In contrast to the canonical ensemble MC (CEMC) simulations, they considered an open system in the *PVT* ensemble. To generate droplets containing up to 450 molecules and to calculate their free energy, the authors employed the umbrella sampling technique.[26,27] The sampling of molecular configurations was biased to favor formation of clusters by introducing a fictitious potential. The size dependence of the droplet free energy was derived from the droplet size distribution. Different other methods based on a combination of biased MC simulations in different ensembles and umbrella sampling were later introduced and successfully employed to study nucleation in LJ fluid and more complex systems, particularly by Kusaka[28,29] and Chen *et al.*[30] These methods are the best currently available. Although the umbrella sampling technique has a rigorous statistical mechanical foundation and its computational efficacy can be significantly improved,[30] the biasing potential depends on an accepted definition of molecular clusters which has a geometrical rather than a thermodynamic nature. Review of cluster criteria may be found in Ref. 31. Merikanto *et al.*[32] explored the influence of neighbor cutoff distances for Stillinger's criterium[33] on the size and free energy of very small water clusters (less than 20 molecules); however, comprehensive studies of the cluster criteria for larger clusters are still lacking.

In this work, we employ a new rigorous scheme of MC simulations, first introduced for studies of the nucleation of liquid bridges and bubbles in cylindrical capillaries in our previous paper.[34] Similarly to the LBA approach, we study LJ droplets confined to a finite volume spherical cell. However, our MC simulation approach is free of the shortcomings of the techniques discussed above. The paper is structured as follows: In Sec. II we present the results of MC simulation. We generate a series of clusters of different sizes using the gauge cell simulation method.[35,36] The gauge cell method allows us to determine directly the chemical potential of clusters without making any assumptions about the cluster geometry or using the virial. The cluster size is defined thermodynamically through the excess number of molecules in the droplet state with respect to the maternal vapor state. We show that the constructed excess isotherm of critical nuclei does not depend on the size of the simulation cell.

The nucleation barrier is defined as the differences of the grand thermodynamic potentials of the droplet state and the

vapor state at a given chemical potential. Integration along the excess isotherm gives the variation of the nucleation barrier with the droplet size according to a general thermodynamic integration formula stemmed from the nucleation theorem.[37–39] Because the isotherm of the droplet states cannot be constructed in the region of very small clusters, which are inherently unstable and thus cannot be continuously connected with the vapor state, the nucleation barrier of one reference droplet has to be estimated independently. To this end, we invoke the ghost field method, introduced in Ref. 34. Within this method, a reference droplet is constructed in a continuous fashion, thus allowing for thermodynamic integration to determine the droplet grand thermodynamic potential. The droplet is formed in an external ghost field of tunable magnitude, which is then removed. We show that the magnitude of the ghost field does not affect the result of thermodynamic integration. The combination of the gauge cell method and the ghost field method provides a rational for rigorous calculations of the droplet free energy, and respectively, the droplet surface tension. Ghost field method and simulation details are described in Sec. II. In Sec. III we compare the results obtained by MC simulations with the pressure tensor method and the capillarity approximation and Tolman equations. We perform MD simulations to calculate the surface tension in accord with the RB method[3] and confirm the conclusion made earlier by ten Wolde and Frenkel[21] about an apparent inconsistency of the pressure tensor calculations in small clusters. We show that the capillarity approximation, which employed the equation of state of Johnson *et al.*[40] for LJ fluid, provides a reasonable approximation for the droplet isotherm. However, its accuracy is not sufficient to predict quantitatively the nucleation barrier which is very sensitive to minor variations of the surface tension. The droplet surface tension can be fitted by the Tolman equation[7] only for relatively large droplets of radius exceeding four molecular diameters. For smaller droplets, which are indeed of special interest for predicting the rate of nucleation in a metastable vapor, the deviations are unacceptable for practical estimates. Finally, in Sec. IV we summarize our main conclusions.

II. MONTE CARLO SIMULATIONS

A. Simulation details: The gauge cell method

The surface tension, which is the most important parameter in nucleation theory, is so sensitive to the details of simulations that the scatter of data reported in the literature is not surprising. In this work we simulate LJ fluid with no cutoff at a subcritical temperature, $kT/\varepsilon=0.7625$. We chose the uncut LJ fluid because of a reasonable consistency of the planar surface tension γ_∞ reported by different researches who used various methods with and without explicit simulation of the vapor-liquid interface.[30,41–44] The comparison of the literature data is given in Fig. S1 (supplemental information).[45] At $kT/\varepsilon=0.7625$, interpolation of the published results (we considered that γ_∞ changes linearly with $1/T$) vary from $0.99\varepsilon/\sigma^2$ (Ref. 41) to $1.02\varepsilon/\sigma^2$.[30,43] Unless otherwise stated, we use the value of $\gamma_\infty=1.02\varepsilon/\sigma^2$ reported in Refs. 30 and 43 while comparing the simulation results with the results of the capillarity approximation.

We performed MC simulations of the vapor-to-droplet transition in LJ fluid confined to a spherical cell with a repulsive wall to prevent heterogeneous condensation. The isotherm of the metastable vapor was generated by the grand canonical ensemble MC (GCMC) method .[46] The isotherm of droplets, which are unstable in an open system, was generated using the gauge cell method.[35,36] In this method, the system is considered in the chemical equilibrium with the gauge cell that represents a finite volume reservoir. The limited capacity of the gauge cell constrains the density fluctuations in the system and allows one to stabilize the labile states such as critical nuclei and to determine their chemical potential. The original procedure[35,36] was modified: the fluid-fluid interactions in the gauge cell were omitted and the fluid in the gauge cell was considered as the ideal gas similarly to the standard GCMC simulation scheme.[47]

The isotherm constructed by the gauge cell method corresponds to the canonical ensemble isotherm of droplet states. It is presented as a dependence of the total number of molecules or loading N_d on the chemical potential μ. The chemical potential at a given loading N is defined as the increment of the Helmholtz free energy upon insertion of one additional molecule, namely,

$$\mu(N_d) = F_d(N_d + 1) - F_d(N_d). \tag{5}$$

In so doing we do not invoke any assumptions regarding the vapor pressure or using the virial equation, which is not justified for such small systems.[9] For the details of the gauge cell method we refer to Refs. 35 and 36.

In order to extend the simulations into the region of high pressures and small cluster diameters and to verify the method consistency, we employed two cells of sizes $R_c=11\sigma$ and 9σ. The wall exerted r^{-12}-type repulsive potential to prevent heterogeneous condensation, so that the effective cell radii were 10σ and 8σ correspondingly. The Markov chains were as long as about 10^6 MC steps per molecule. Each step included attempts of molecule insertion, displacement, and removal from the cell (in the grand canonical ensemble and the gauge cell method alike). The gauge cell volume was chosen to have in average no less than 16 molecules. At this condition, as we cautiously checked, the histograms of the numbers of particles in the cells are symmetric, and, thus, the chemical potential can be reliably derived from the average number of molecules in the gauge cell.

In MC simulations, we did not impose any restrictions on the location of the cluster center of mass, in contrast with the classical papers of LBA (Ref. 1) and RB,[3] where the cluster was kept in the center of the simulation cell. As shown by Reiss, Katz, and Cohen (RKC)[48] and Oh and Zeng,[49] these restrictions may affect the free energy estimate considerably. According to the terminology of Ref. 49 the droplets we simulate are RKC clusters rather than LBA clusters.

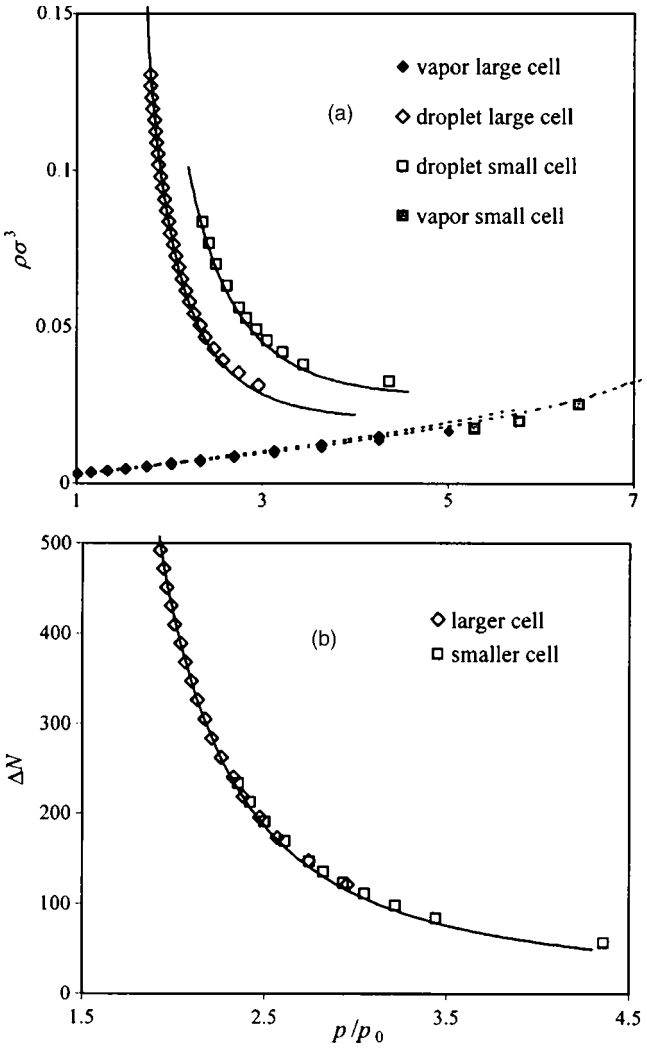

FIG. 1. MC isotherms of droplet and vapor configurations: (a) full isotherms; (b) excess isotherm of droplets. Squares, 9σ (smaller) cell; diamonds, 11σ (larger) cell. Open symbols denote droplet states; closed symbols denote vapor states. Dotted lines correspond to the equation of state of Johnson *et al.*[40] for the vapor phase. Solid lines show the predictions of the capillarity approximation calculated with $\gamma_\infty = 1.02\varepsilon/\sigma^2$ and the equation of state of Johnson *et al.* for LJ fluid.

B. Excess isotherms of LJ clusters

Figure 1(a) shows the isotherms of droplet configurations $N_d(s)$ obtained using the gauge cell method. All droplet configurations consisted of one liquidlike cluster surrounded by vapor. Due to a small size of the simulation cell, multiple clusters were not observed. The isotherm is given as the fluid density in the cell, $\rho = N/V$ (N is the loading and V is the cell volume) being a function of the supersaturation $s = p_v/p_0$. The latter was calculated from the chemical potential μ determined in the gauge cell. As the number of molecules in the system decreases, the droplet becomes smaller and the vapor pressure increases. At a certain point, the droplet configuration becomes unstable, and the fluid undergoes an irreversible transition to a vapor state. This behavior is characteristic for any finite volume subcritical system sufficiently distant from the critical point.[10] In the larger cell, the fluid underwent the droplet-to-vapor transition at the loading $N_c = 220$; in the smaller cell the transition occurred at $N_c = 115$. The vapor isotherms $N_v(s)$ in two cells practically coincide [Fig. 1(a)].

The excess isotherm is calculated as the difference of the droplet and vapor isotherms, $\Delta N_d(s) = N_d(s) - N_v(s)$. In Fig. 1(b), the excess isotherm is plotted as the excess number of molecules in the cluster as a function of the supersaturation s. The excess isotherms obtained in two cells excellently merge at $p_v/p_0 = 2.4$–3.0, thus confirming the consistency of the gauge cell method. Combining the results obtained in both cells that spans the range of cluster sizes from 65 to 500 molecules we get a "unified" excess isotherm, which approximately corresponds to the range of droplet radii from 2.5 to 6.5 molecular diameters.

The droplet stabilized in the close system using the gauge cell method corresponds to the critical nucleus in an open system at the same chemical potential. Indeed, let us recall that the critical nucleus is defined from the condition of the maximum work of droplet formation. The work of formation of the droplet state of loading N from the maternal metastable vapor phase confined to the volume V at given chemical potential μ and temperature T is equal to the free energy difference between the droplet and vapor states minus the loading difference times μ:

$$\Delta W(N,\mu) = F_d(N) - F_v[N_v(\mu)] - [N - N_v(\mu)]\mu. \tag{6}$$

Note that $\exp[-\Delta W(N,\mu)/kT]$ determines the probability of observation of the state of loading N in the grand canonical ensemble at a given chemical potential μ. The state of critical nucleus in the open system has the minimal probability of observation that corresponds to a maximum of $\Delta W(N,\mu)$ with respect to N at a given μ. The condition of maximum is fulfilled for the droplet state $N = N_d$, the chemical potential of which $\mu(N_d)$ satisfies the inequality,

$$F_d(N_d+1) - F_d(N_d) = \mu(N_d) < \mu < \mu(N_d-1) = F_d(N_d) - F_d(N_d-1), \tag{7}$$

which follows from the definition of the chemical potential (5). For relatively large loadings, which are characteristic for the systems considered here, the condition (7) reduces to the conventional condition of chemical equilibrium between the droplet and vapor states,

$$\left.\frac{\partial F_d(N)}{\partial N}\right|_{N=N_d} = \mu(N_d) = \mu. \tag{8}$$

Thus, the droplet isotherm $N_d(\mu)$ corresponds to the states of critical nuclei, and constructed in Fig. 1(b) excess isotherm, $\Delta N_d(s) = N_d(s) - N_v(s)$, represents the isotherm of critical nuclei.

In Fig. 1, we also present the predictions of the capillarity approximation for the droplet-vapor equilibrium in the LJ fluid using the equation of state of Johnson *et al.*,[40] which related equilibrium bulk vapor and liquid densities $\rho_{1/v}$ and pressures $p_{1/v}$ to the chemical potential μ. This equation agrees with the vapor phase simulation [dotted lines in Fig. 1(a)]. To calculate the droplet isotherm

$$N_d(\mu) = \rho_v(\mu)V_{\text{cell}} + \tfrac{4}{3}\pi r^3[\rho_l(\mu) - \rho_v(\mu)], \tag{9}$$

the droplet radius r was calculated by the Laplace equation, in which the liquid and vapor pressures were calculated using the equation of Johnson *et al.* and the surface tension was assumed equal to its planar value of $1.02\varepsilon/\sigma^2$. The second summand in the right-hand side of Eq. (9) corresponds to the excess isotherm. Note that although we do not employ here any approximations such as those of ideal vapor and incompressible liquid, Eq. (9) cannot be considered flawless. The equimolar droplet radius is substituted by the radius of tension implied by the Laplace equation (2), thus ignoring the difference between planar and curved interfaces. The visual agreement of the capillarity approximation and MC simulation for the cluster isotherms, as well as for the excess isotherm, looks excellent. However, the capillarity approximation, as shown below, fails to quantitatively predict MC simulation results for more sensitive parameters such as the droplet surface tension and the nucleation barrier at a given supersaturation with necessary accuracy.

C. Calculations of the nucleation barrier: The ghost field method

The nucleation barrier $\Delta\Omega_d$ is defined as the work of formation of the critical nucleus in the maternal metastable vapor phase kept at a given chemical potential μ. $\Delta\Omega_d$ corresponds to the maximum work of cluster formation $\Delta W(N,\mu)$ defined by Eq. (6). As shown above, the critical nuclei correspond to the clusters in the droplet states $N_d(\mu)$ generated by the gauge cell method. Thus, the nucleation barrier $\Delta\Omega_d$ can be written as the difference of the grand thermodynamic potentials of the droplet state $N_d(\mu)$ and of the respective vapor state $N_v(\mu)$ at the same chemical potential μ,

$$\Delta\Omega_d(\mu) = \Delta W[N_d(\mu),\mu] = \Omega_d(\mu) - \Omega_v(\mu). \tag{10}$$

Here, the grand thermodynamic potentials of the droplet and vapor states are defined as

$$\begin{aligned}\Omega_d(\mu) &= F_d[N_d(\mu)] - \mu N_d(\mu),\\ \Omega_v(\mu) &= F_v[N_v(\mu)] - \mu N_v(\mu).\end{aligned} \tag{11}$$

Strictly speaking, this definition is restricted to the discrete set of chemical potentials μ_N, which correspond to integer values of N. However, for sufficiently large N we can operate with interpolated functions $N_d(\mu)$ and $N_v(\mu)$ without a loss of the precision.

Integration along the excess isotherm gives the variation of the nucleation barrier with the droplet size according to the general thermodynamic integration relation, which stems from the so-called nucleation theorem,[38,39]

$$\Delta\Omega_d(\mu) = \Delta\Omega_d(\mu_R) - \int_{(\mu_R)}^{(\mu)} \Delta N_d(\mu)\,d\mu. \tag{12}$$

Here, $\Delta\Omega_d(\mu_R)$ is the nucleation barrier for the critical nucleus at a certain chemical potential μ_R that serves as a reference state $\mathbf{D_R}$. Thus, in order to calculate the nucleation barrier for critical nuclei of different sizes it is sufficient to determine the nucleation barrier of one reference droplet. Because the isotherm of the droplet states cannot be continued into the region of very small clusters, which are inherently unstable, and terminates abruptly, the nucleation barrier of the reference droplet has to be estimated independently.

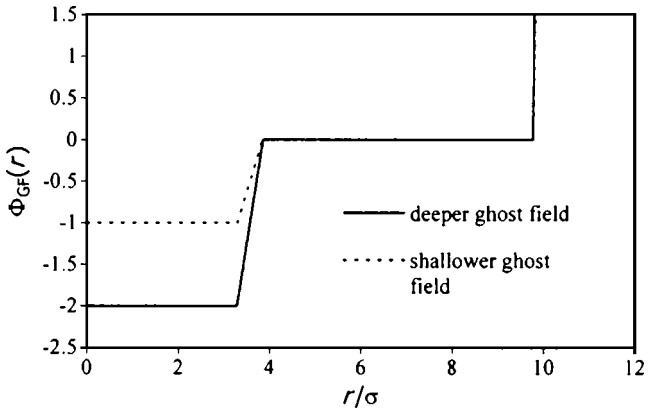

FIG. 2. The profiles of the ghost field potentials (-2ε deeper well, -1ε shallower well) employed for computing the free energy of a reference droplet in 116 cell.

To calculate the nucleation barrier of the reference droplet, we employ the ghost field method introduced recently.[34] This method allows us to construct a continuous trajectory of equilibrium (in the canonical ensemble, close system) states, which connects the reference droplet state $\mathbf{D_R}$ with the respective vapor state $\mathbf{V_R}$, and to calculate the droplet free energy by thermodynamic integration. The technical details of the ghost field method as related to the simulation of droplet nucleation are given elsewhere.[12] The reference droplet is formed in a continuous fashion being stabilized by an external ghost field $\Phi_{\text{ext}}(\mathbf{r}) = \zeta\Phi_G(\mathbf{r})$ of tunable magnitude ζ. The ghost field $\Phi_G(\mathbf{r})$ represents a potential well located in the center of our spherical cell, which facilitates the droplet condensation. In this work, we use two different ghost fields for each system to demonstrate the method consistency. The potential profiles of the ghost field in the 11σ cell are shown in Fig. 2. They differ in the depths of the potential well, $-1kT$ and $-2kT$, respectively. The well is smoothened by the transition zones in order to avoid the potential discontinuity.

We construct the auxiliary isotherm $N_G(\mu)$ of the droplet equilibrated in the ghost field of the maximum magnitude $\zeta=1$ using the gauge cell method. The isotherms build in two potential wells in 11σ cell are presented in Fig. 3. The isotherms have a characteristic sigmoid shape that is typical for capillary condensation in small pores.[36] As the chemical potential increases vapor condenses in the potential well forming a pinned droplet. As expected, condensation in $2kT$ well occurs at lower pressures than in $1kT$ well. The use of the gauge cell method allows us to avoid spontaneous condensation that would be observed in the GCMC method. After condensation, the droplet grows as the chemical potential increases further, and at a certain chemical potential μ_R^* we arrive at a droplet state $\mathbf{G_R^*}$ which contains the same number of molecules as the reference droplet state $\mathbf{D_R}$: the loading $N_G(\mu_R^*) = N_d(\mu_R) = N_R$.

The scheme to build a continuous path connecting the reference droplet state $\mathbf{D_R}$ and the respective vapor state $\mathbf{V_R}$

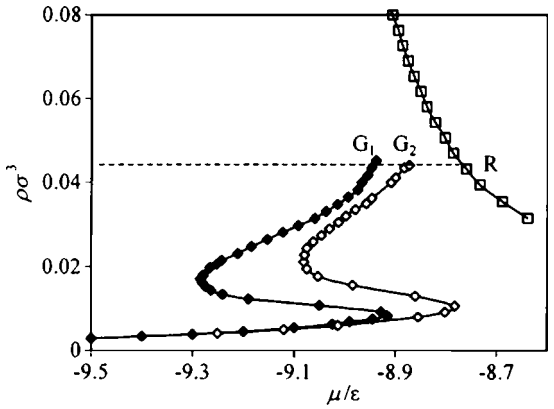

FIG. 3. Isotherms of growing droplets stabilized in the full scale ghost field, $\zeta=1$ (closed diamonds, -2ε potential well; open diamonds, -1ε potential well), and the isotherm of undisturbed droplets, $\zeta=0$, from Fig. 1 (squares). 11σ cell. R is the target reference droplet state at $\mu=\mu_R$. G_1 and G_2 are, respectively, the droplet states of the same density as state R constructed in the ghost field. States G_1 and G_2 are connected with state R by a trajectory of states of equal density (indicated by the horizontal dashed line) generated in a series of CEMC simulations by varying the host field magnitude ζ from 1 to 0.

is illustrated in Fig. 4, where we use the logarithmic scale for loading N for the sake of clarity. The path consists of four segments.

First. Since due to inherent instability of small clusters we cannot continuously grow the critical nucleus starting form the vapor state $\mathbf{V_R}$ by increasing the loading, we reduce the loading along the vapor isotherm $N_v(\mu)$ and arrive at a vapor state $\mathbf{V}_0$ of a low density N_0 at the chemical potential μ_0. The Helmholtz free energy difference between states $\mathbf{V_R}$ and $\mathbf{V}_0$ is calculated as

$$F_v[N_v(\mu_R)] - F_v(N_0) = \int_{(N_0)}^{(N_{VR})} \mu dN_v. \tag{13}$$

For small loadings the integral is replaced by a sum.

Second. We turn on the ghost field and incrementally increase its magnitude ζ from 0 (state $\mathbf{V}_0$) to 1 (state $\mathbf{G}_0$ on the ghost field isotherm at the chemical potential μ_0^*) keeping the loading fixed, $N_G(\mu_0^*)=N_d(\mu_0)=N_0$. In doing so we construct a series of vapor states in the canonical ensemble by varying the ghost field magnitude ζ. The corresponding trajectory of states of equal loading, $\mathbf{V}_0\mathbf{G}_0$, which we call N_0 isostere, constitute the second segment. As shown in Ref. 34, the Helmholtz free energy difference between states $\mathbf{V}_0$ and $\mathbf{G}_0$ is calculated by the integration along N_0 isostere from $\zeta=1$ to $\zeta=0$,

$$F_v(N_0) - F_G(N_0) = -\int_0^1 \langle \Phi_G \rangle_{N_0,\zeta} d\zeta. \tag{14}$$

Here, $\langle \Phi_G \rangle_{N_0,\zeta}$ denotes the canonical ensemble average of the ghost field potential $\Phi_G(\mathbf{r})$ for the fluid of loading N_0 equilibrated in the ghost field of magnitude ζ. $\langle \Phi_G \rangle_{N_0,\zeta}$ is calculated by weighting the ghost field potential along N_0 isostere with the average fluid density $\rho_{N_0,\zeta}(\mathbf{r})$ in the ghost field of the magnitude ζ:

$$\langle \Phi_G \rangle_{N_0,\zeta} = \int_V \Phi_G(\mathbf{r}) \rho_{N_0,\zeta}(\mathbf{r}) d^3\mathbf{r}. \tag{15}$$

Derivation of Eq. (14) is given in the Appendix.

Equations (14) and (15) imply numerical integration whose accuracy depends on the number of canonical ensemble simulations at different $\zeta=1,\ldots,\zeta_i,\zeta_{i+1},\ldots,0$. When the loading is so small that the fluid can be considered as ideal gas and fluid-fluid interaction is negligible, the Helmholtz free energy difference between states $\mathbf{V}_0$ and $\mathbf{V}_0^*$ is equal to $N_0(\mu_0-\mu_0^*)$.

Third. The ghost field isotherm $N_G(\mu)$ connects vapor state $\mathbf{G}_0$ and droplet state $\mathbf{G_R}$ at a chemical potential μ_R^*, which contains the desired number of molecules $N_G(\mu_R^*)=N_d(\mu_R)=N_R$. The Helmholtz free energy difference between states $\mathbf{G}_0$ and $\mathbf{G_R}$ is calculated as

$$F_G(N_0) - F_G(N_R) = -\int_{(N_0)}^{(N_{VR})} \mu dN_G. \tag{16}$$

Fourth. The ghost field is gradually removed incrementally decreasing the field magnitude ζ from 1 to 0 in a series

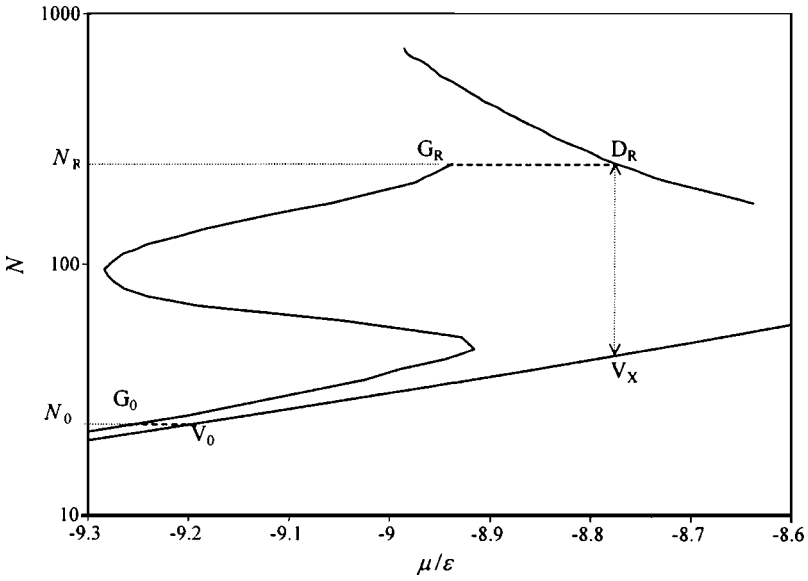

FIG. 4. Calculating the Helmholtz free energy and nucleation barrier for the reference droplet (results of simulation in 11σ cell and 2.0ε ghost field). Continuous trajectory of states connecting vapor state $\mathbf{V_R}$ and droplet state $\mathbf{D_R}$ at chemical potential μ_R consists of four segments: (1) vapor isotherm $\mathbf{V_R}\mathbf{V}_0$ (the number of molecules is reduced from N_R to N_0); (2) ghost field isostere $\mathbf{V}_0\mathbf{G}_0$ of constant loading N_0 (the ghost field magnitude is increased from $\zeta=0$ to $\zeta=1$ in the canonical ensemble); (3) ghost field isotherm $\mathbf{G}_0\mathbf{G_R}$ (the number of molecules is increased from N_0 to N_R); (4) ghost field isostere $\mathbf{G_R}\mathbf{D_R}$ of constant loading N_R (the ghost field magnitude is decreased from $\zeta=1$ to $\zeta=0$ in the canonical ensemble).

of canonical ensemble simulations keeping the number of molecules in the system unchanged, $N=N_R$. The isostere, thus constructed, connects droplet state $\mathbf{G_R}$ equilibrated in the ghost field and desired reference droplet state $\mathbf{D_R}$. Along the isostere, the droplet partly evaporates and the chemical potential increases at the isothermal conditions from $\mu=\mu_R^*$ at $\zeta=1$ (state $\mathbf{G}$) to $\mu=\mu_R$ at $\zeta=0$ (state $\mathbf{D_R}$).

Similarly to Eq. (14), the Helmholtz free energy difference between states $\mathbf{G_R}$ and $\mathbf{D_R}$ is calculated by the integration along N_0 isostere from $\zeta=1$ to $\zeta=0$,

$$F_G(N_R) - F_d(N_R) = \int_0^1 \langle \Phi_G \rangle_{N_R,\zeta} d\zeta. \tag{17}$$

Here, $\langle \Phi_G \rangle_{N_R,\zeta}$ denotes the canonical ensemble average of the ghost field potential $\Phi_G(\mathbf{r})$ for the fluid of loading N_0 equilibrated in the ghost field of the magnitude ζ. $\langle \Phi_G \rangle_{N_R,\zeta}$ is calculated by weighting the ghost field potential along N_R isostere with the average fluid density $\rho_{N_r,\zeta}(\mathbf{r})$ in the ghost field of the magnitude ζ:

$$\langle \Phi_G \rangle_{N_0,\zeta} = \int_V \Phi_G(\mathbf{r}) \rho_{N_R,\zeta}(\mathbf{r}) d^3\mathbf{r}. \tag{18}$$

Thus, the desired Helmholtz free energy difference between states $\mathbf{D_R}$ and $\mathbf{V_R}$ is given by

$$F_d(N_R) - F_v[N_R(\mu_R)] = -\int_{(N_0)}^{(N_{\mathcal{VR}})} \mu dN_v + \int_0^1 \langle \Phi_G \rangle_{N_0,\zeta} d\zeta + \int_{(N_0)}^{(N_R)} \mu dN_G - \int_0^1 \langle \Phi_G \rangle_{N_R,\zeta} d\zeta. \tag{19}$$

Finally, the nucleation barrier of the reference droplet $\mathbf{D_R}$ required in Eq. (6) is determined in accord to Eq. (10) as

$$\Delta\Omega_d(\mu_R) = \Omega_d(\mu_R) - \Omega_v(\mu_R) = F_d(N_R) - F_v[N_R(\mu_R)] - \mu_R \Delta N_d(\mu_R). \tag{20}$$

The calculation of the free energy difference along the isoteres $\mathbf{V_0G_0}$ and $\mathbf{G_RD_R}$ is worth special comments. The integral in Eq. (16) along the vapor states equilibrated at different ζ since the intermolecular interactions are insignificant and the system behaves as an ideal gas in the external field. Ideal gas approximation $\int_0^1 \langle \Phi_G \rangle_{N_0,\zeta} d\zeta \approx N_0(\mu_0 - \mu_0^*)$ works with the accuracy of $0.3kT$. The most computationally demanding operation is the calculation of the free energy difference along the isotere $\mathbf{G_RD_R}$. The calculation of $\langle \Phi_G \rangle_\zeta$ is demonstrated in Fig. 5, where we plot $\langle \Phi_G \rangle_\zeta$ against the ghost field magnitude ζ. The contribution of the ghost field to the free energy $F(N_R)$ is calculated by integration of $\langle \Phi_G \rangle_\zeta$, Eq. (17). When the ghost field is relatively strong ($\zeta > 0.05$) the cluster is pinned to the potential well and is located in the center of the cell. The statistical weight of configurations with the cluster located on the cell periphery is vanishingly small, although there is no restriction on the location of the center of mass. When ζ approaches zero, practically any location of the cluster in the cell is equally probable. Then, $\langle \Phi_G \rangle_\zeta$ varies rapidly and the precision of the free energy estimate depends on the quality of simulations at small ζ. Note that while $\langle \Phi_G \rangle_\zeta$ is of the order of $10kT$ and even $100kT$, the desired uncertainty of the nucleation barrier calculations is at most several kT. In order to facilitate sampling at $\zeta < 0.02$, we used a special type of MC move shifting all molecules in the cell along the same randomly chosen vector of length less than 0.1σ.

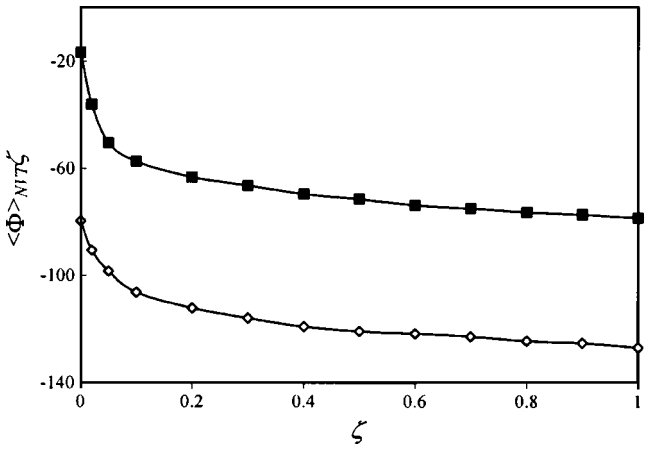

FIG. 5. Calculation of the contribution of the ghost field into the Helmholtz free energy: $\langle \Phi_G \rangle$ for 11σ (open symbols) and 9σ (closed symbols) cells as a function of the ghost field magnitude ζ, Eq. (9).

Via long (10^6 steps) simulations we achieved the desired precision of the nucleation barrier calculations. We estimate that 90% confidence level corresponds to $\approx \pm 1.5kT$ for the larger cell and $\pm 0.75kT$ in the smaller cell. These estimates are confirmed by a very reasonable agreement between the barriers obtained in different cells via independent series of simulations performed with the different ghost fields. The difference between the results of the two series was $1.9kT$ for the larger cell and $1.3kT$ for the smaller cell.

Figure 6(a) shows the calculated nucleation barriers as a function of the relative vapor pressure, which represents the average of the four independent simulation series. The arrows show the states, which were employed as the target reference droplet states in the ghost field method, in the larger and smaller cells. The precision of free energy calculations in the ghost field method is demonstrated in Fig. 7, where we present the work of formation of the droplet state of loading N from the maternal metastable vapor phase $\Delta W(N,\mu)$ defined by Eq. (6) at the chemical potential $\mu = \mu_R$. The maximum of $\Delta W(N,\mu)$ is achieved exactly at $N = N_R = N_d(\mu_R)$ and is equal to $\Delta\Omega_d(\mu_R)$ which is indicated by dotted line.

III. DISCUSSION

A. Comparison with the pressure tensor method: Molecular dynamics simulations

Puzzled by a striking disagreement between the biased MC simulation results and the pressure tensor calculations of the cluster free energy reported by ten Wolde and Frenkel,[21] we decided to check this conclusion by performing molecular dynamics simulations exactly in accordance with RB method.[3] The molecules were confined to a spherical cell of $R_c = 11\sigma$. The wall exerted an r^{-12}-type repulsive potential,

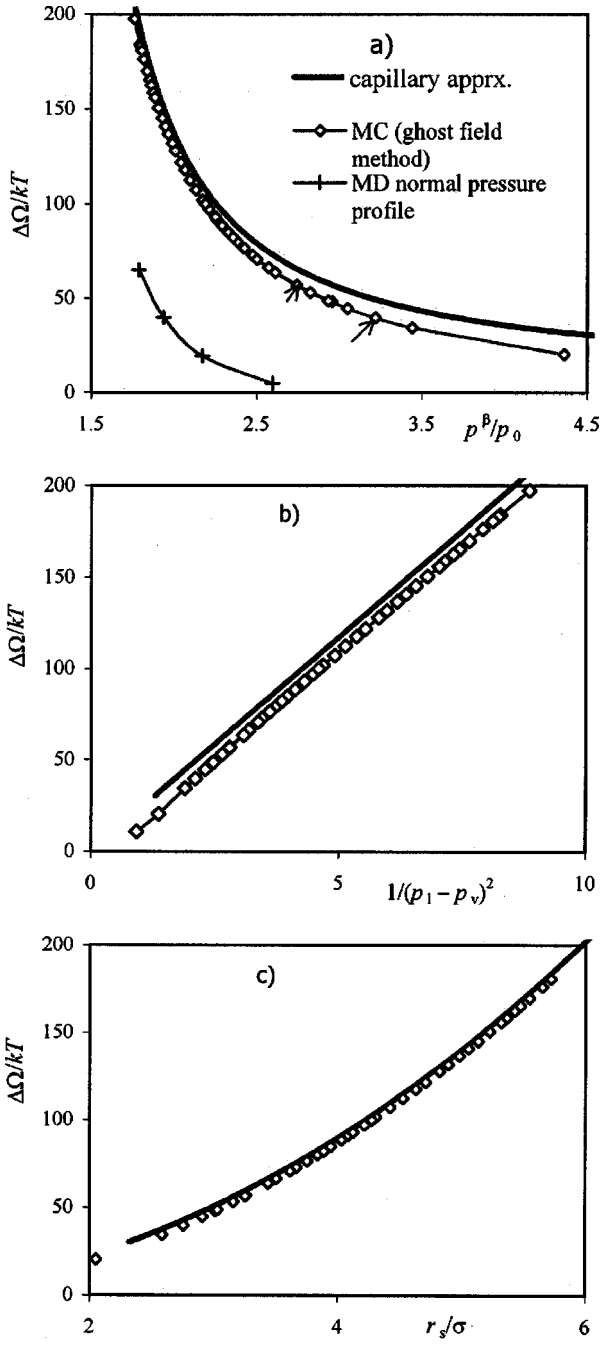

FIG. 6. Nucleation barriers in LJ fluid computed in MC and MD simulations and predicted by the capillarity approximation. The results are presented in different coordinates: (a) as a function of supersaturation (the arrows show the reference states generated in the ghost field in two cells employed in simulations), (b) as a function of reciprocal pressure difference squared (the capillarity approximation implies a linear dependence, (c) as a function of droplet size defined as the radius of tension.

so the effective cell radius was 10σ. We simulated a series of clusters of $N=216$, 343, 512, and 729 molecules. The time step was 10^{-14} s. We performed 1 ns simulation with a primitive velocity-scaling thermostat. After that, a suitable moment was chosen to correct the temperature and the energy, and the simulation was continued for another 10 ns in the microcanonical ensemble. The average temperature was within $0.005kT/\varepsilon$ interval from the target temperature $kT/\varepsilon = 0.7625$.

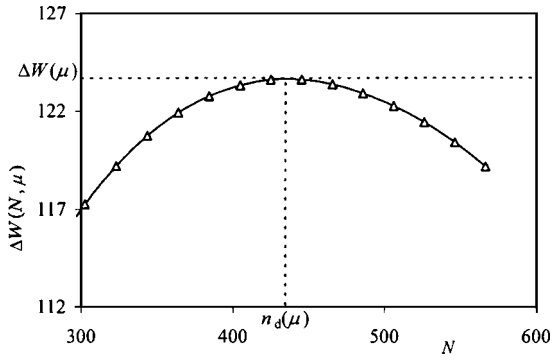

FIG. 7. The work of formation, $\Delta W(N,\mu)$, of the droplet state of loading N from the vapor state at a given chemical potential μ. The nucleation barrier $\Delta\Omega_d(\mu)$ corresponds to the maximum of $\Delta W(N,\mu)$ achieved at the droplet state $N_d(\mu)$ containing the critical nucleus. Calculations are presented for the chemical potential $\mu=-8.9\varepsilon$.

The radial profiles of density, configurational energy, and pressure counted from the center of mass were obtained by averaging over 10 ns microcanonical simulations. They are given in supplementary information, Figs. S2–S4.[45] These profiles are quite typical for the spherical clusters and qualitatively resemble the results published earlier by different authors.[3,16,17,21] The density in the middle of the clusters as well as the internal energy per molecule are approximately equal to that in the bulk liquid, but the pressure in smaller clusters is substantially lower than the expected bulk value. Because it is not possible to evaluate the chemical potential μ directly from MD simulations, we estimated the vapor pressure p_v (and μ) by interpolating the number of molecules in the MD cell onto $N(p_v)$ curve obtained from gauge cell method. The pressures obtained from the densities of the vapor surrounding the cluster were 1%–3% lower, which did not affect the qualitative outcome.

The nucleation barrier defined as the mechanical work of cluster formation was calculated as

$$\Delta\Omega = 2\pi\int_0^\infty [p_n(r) - p_v]r^2 dr, \tag{21}$$

where $p_n(r)$ is the normal pressure component and p^β is the vapor pressure, which was approximated by the pressure at the periphery of the cell. The results are given in Fig. 6(a). The nucleation barriers calculated through Eq. (21) are incomparably lower than those found in MC simulations. Although we did not expect to find such dramatic difference, this result agrees with the conclusion of ten Wolde and Frenkel.[21] Thus, we confirm that the pressure tensor method, which is justified for macroscopic interfaces, is not applicable for small clusters of molecular dimensions.

B. Comparison with the capillarity approximation and Tolman equations

There are different ways to compare the simulation results with the capillarity approximation. The practical question to be addressed is "How good does the capillarity approximation of the classical nucleation theory predict the nucleation barrier and, respectively, the rate of nucleation at a given supersaturation?" In this respect, the nucleation bar-

rier has to be presented as a function of the vapor pressure or the chemical potential. In Fig. 6(a), we present the nucleation barriers calculated as a function of the relative pressure in accord with Eq. (1) in the form $\Delta\Omega_d = 16\pi\gamma_s^3/(3\Delta p^2)$, in which the pressure difference Δp was obtained by using the equation of state for the LJ fluid given by Johnson *et al.*,[40] and the planar surface tension of $1.02\varepsilon/\sigma^2$. The capillarity approximation seems to give a reasonable estimate of the nucleation barrier with deviations from the MC simulation results from ~ 5 to $\sim 10kT$. However, these deviations exceed the requirements for realistic predictions of the rate of nucleation which is the primary practical goal of a quantitative nucleation theory. Indeed, the rate of nucleation is proportional to $\exp(-\Delta\Omega_d/kT)$. This means that $\sim 10kT$ error in the nucleation barrier produces an error of $\sim 10^4$ in the estimate of nucleation rate which is hardly acceptable. The difference between the simulation results and the capillarity approximation is clearly seen in Fig. 6(b), which presents the results in coordinates $\Delta\Omega - 1/(\Delta p)^2$. In these coordinates, the capillarity approximation gives a straight line with the slope proportional to the assumed surface tension cubed. The MC plot is almost parallel to the straight line predicted by the capillarity approximation in agreement with suggestions of McGraw and Laaksonen[50,51] and the simulation of ten Wolde and Frenkel.[21] However, the deviation from the constant offset does indeed matter and reflects the dependence of the droplet surface tension on the droplet size. Note that the precision of our MC simulation approach was estimated within $(1-2)kT$, which makes the simulation results suitable for the quantitative predictions of the rate of nucleation.

The nucleation barrier, calculated in the capillarity approximation at a given supersaturation, is extremely sensitive to the assumed value of the surface tension due to the cubic dependence. It is possible to reduce the deviations from the MC results by fitting the surface tension; however, this approach would be misleading for the real dependence of the surface tension on the droplet size were masked with a "suitable" value.

It seems natural to present the nucleation barrier as a function of the droplet size in accord with the Gibbs equation (1), $\Delta\Omega_d = (4\pi/3)r_s^2\gamma_s$, which is a linear function of the surface tension. The nucleation barriers, as functions of the surface of tension radius r_s, are given in Fig. 6(c). The deviations between the MC results and the capillarity approximation are reduced as compared to the plots in Fig. 6(b) by about a factor of 3. However, this is a somewhat deceptive agreement since the capillarity approximation implies a different droplet size than the simulation, which depends on the assumed surface tension. Thus, the plots in Fig. 6(c) compare the droplets corresponding to different vapor pressures.

From the excess grand thermodynamic potential $\Delta\Omega$ calculated in MC simulations and the MC equation of state for bulk phases that determines the pressure difference, $\Delta p = p^\alpha - p^\beta$, at a given chemical potential, one can define the radius of tension r_s and the corresponding surface tension γ_s resolving Eq. (1), respectively. In Fig. 8 we present the relation between the surface tension and the droplet radius calculated from the MC data. The surface tension monotonically increases with the droplet size smoothly approaching the planar limit shown with the solid line. For droplets as large as six molecular diameters, which contain about 10^3 molecules, the surface tension differs from the planar surface tension by $\sim 2\%$. The deviation progressively increases as the droplet size decreases and constitutes $\sim 15\%$ for droplet of 2σ radius, which contain 60 molecules. We attempted to approximate the simulation results with the Tolman equation with Eq. (4). The results of the fit with the planar surface tension $\gamma_\infty = 1.02\varepsilon/\sigma^2$ and the Tolman length $\delta = 0.05\sigma$ is given in Fig. 6. There is reasonable agreement in the range of droplets exceeding 4σ radius and correspondingly ~ 300 molecules. The planar surface tension interpolated by the Tolman equation perfectly agrees with the data of Errington[43] and Chen *et al.*[30] For smaller droplets, deviations progressively increase. It was not possible to extend its applicability to a larger diapason of droplet radii by varying the parameters of Eq. (3).

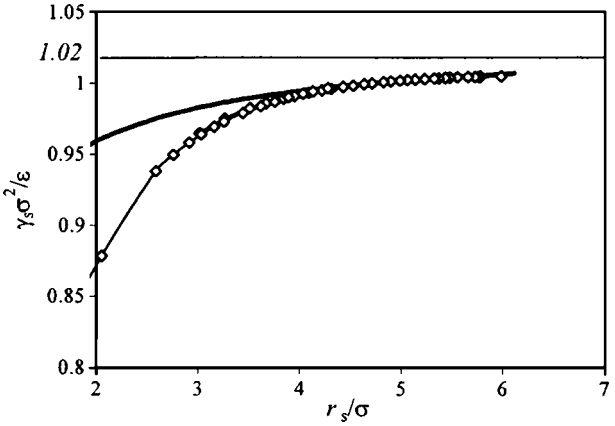

FIG. 8. Size dependence of the surface tension. The bold line shows a fit to the Tolman equation (4) with the constant Tolman length of 0.05σ and the planar value of surface tension $\gamma_\infty = 1.02\ \varepsilon/\sigma^2$ marked by the horizontal line. The fit is valid for droplets larger 4σ.

IV. CONCLUSIONS

We employed a new rigorous approach to simulate homogeneous droplet nucleation, which allows for calculating the free energies of clusters with precision of $(1-2)kT$. We simulated a series of clusters ranging in radius from 2σ to 6σ and containing, respectively, from ~ 50 to ~ 500 molecules. We studied LJ fluid with no cutoff, for which the planar surface tension was determined accurately in recent simulations.[30,41,43] The temperature of simulation was chosen $kT/\varepsilon = 0.7625$ that corresponds to the boiling temperature of the LJ model of nitrogen.[52] The clusters were simulated as confined to a spherical cell with slightly repulsive walls to avoid heterogeneous nucleation. Two parallel simulations in the cells of different radii were performed to demonstrate the independence of simulation results on the size of the simulation cell. The analysis was performed in a purely thermodynamic fashion in terms of excess quantities, namely, the excess cluster mass and the excess cluster free energy, without invoking any assumption about cluster geometry or vapor ideality. The clusters were generated by means of the gauge cell method,[35] in which the chemical potential of the

cluster is measured directly. The simulated isotherm of droplet states cannot be continuously connected with a vapor state due to the inherent instability of very small clusters. This discontinuity of the droplet isotherm does not allow for computing absolute values of the droplet free energy, although the relative values with respect to a selected reference droplet state can be calculated by integration along the isotherm in accord with the general thermodynamic relation (6). We employed the ghost field method introduced in our previous paper[34] to construct a continuous trajectory of states connecting a selected droplet state and a low density vapor state to compute the droplet free energy by the thermodynamic integration along this trajectory. Two parallel simulations with different depths of the ghost field were performed to demonstrate the method consistency and to estimate the uncertainty of the free energy calculations.

The combination of the gauge cell method and the ghost field method provides a precise technique for simulations of critical nuclei and calculations of the excess free energy, which is immediately related to the nucleation barrier and the droplet surface tension. We constructed the dependence of the surface tension on the droplet radius of tension. The surface tension increases monotonically and approaches the planar value of $\gamma_\infty = 1.02\varepsilon/\sigma^2$, reported in the recent papers of Errington[43] and Chen *et al.*[30]

The data obtained were used to check the limits of applicability of the capillarity approximation for evaluation of the free energies of small liquid droplets. To avoid common assumptions of vapor ideality and liquid incompressibility, we invoked the MC equation of state of LJ fluid given by Johnson *et al.*[40] to calculate the droplet isotherm and the nucleation barrier according to the Eqs. (1) and (2) using the planar value of $\gamma_\infty = 1.02\varepsilon/\sigma^2$. We found that this most precise version of the capillarity approximation provided a reasonable fit of the droplet isotherm; however, the deviations between the nucleation barriers varied from $\sim 5kT$ to $\sim 10kT$ far exceeding estimated errors of the simulation results. We checked also the applicability of the Tolman equation (4) to quantitatively predict the droplet surface tension. A suitable fit was found for droplets larger than 4σ with the constant Tolman length of 0.05σ. For smaller droplets, the Tolman length defined as the difference between the equimolar radius and the radius of tension progressive increased with the decrease of the droplet size.

We performed the MD simulation of the same system to verify the conclusion made by ten Wolde and Frenkel[21] that the mechanical approach based on the calculation of the pressure tensor, which was employed in a number of papers, is inconsistent with the thermodynamic interpretation of the results of MC simulations. To this end, we employed the RB method for computing the pressure profiles across the droplet and calculating the droplet free energy. We found a striking difference between the mechanical and the thermodynamic approaches similar to that reported in Ref. 21. We conclude that our simulation results are qualitatively similar to those obtained by ten Wolde and Frenkel[21] by biased MC simulations performed in the *PVT* ensemble for LJ fluid with the 2.5σ cutoff at $kT/\varepsilon = 0.741$. It worth noting that, elsewhere,[12] we have simulated the system studied in Ref. 21 by the MC approach employed in this work and found a quantitative agreement with the results reported in Refs. 9 and 23. Thus, we confirm that the pressure tensor method, which is justified for macroscopic interfaces, is not applicable when the system size is comparable with the range of intermolecular forces, such as for small clusters of molecular dimensions.

Finally, it is worth noting that the MC simulation approach we developed, based on the combination of the gauge cell method for generating unstable configurations of nuclei and the host field method for calculating nuclei free energies, can be recommended for studies of various nucleation phenomena in nanoscale systems, related to vapor-liquid and liquid-solid transformations between the surfaces and in pores, bubble cavitation, dewetting, tribology, etc.

ACKNOWLEDGMENTS

The work was supported by the TRI/Princeton exploratory research program and the John Simon Guggenheim Memorial Foundation (AVN).

APPENDIX: DERIVATION OF THE CHANGE OF THE FREE ENERGY OF THE SYSTEM IN THE PROCESS OF TURNING ON (OFF) THE EXTERNAL FIELD

To calculate the change of the Helmholtz free energy of the system in the process of turning on (off) the ghost field along the CEMC isostere at *NVT* fixed by varying the ghost field magnitude from $\zeta = 0(1) \rightarrow \zeta = 1(0)$. Let us consider the Helmholtz free energy $F_G(N,\zeta)$ of the fluid in the ghost field of the magnitude ζ. $F_G(N,1) = F_G(N)$ and $F(N,0) = F_{v(d)}(N)$. $F(N,\zeta)$ is defined through the canonical partition function

$$Q(N,V,T,\zeta) = \frac{1}{\Lambda^{3N} N!} \int d\mathbf{r}^N \exp\{-[\Phi(\mathbf{r}^N) + \zeta\Phi_G(\mathbf{r}^N)]/kT\}, \tag{A1}$$

as

$$F(N,V,T,\zeta) = -kT \ln Q(N,V,T,\zeta). \tag{A2}$$

Here, $\Phi(\mathbf{r}^N)$ is the total potential energy of interactions between the molecules and between the molecules and the repulsive wall and $\zeta\Phi_G(\mathbf{r}^N)$ is the potential energy of particle interaction with the ghost field of magnitude ζ. The derivative of F with respect to the host field magnitude is represented as the canonical ensemble average of the ghost field,

$$\left.\frac{\partial F}{\partial \zeta}\right|_{N,V,T} = -kT \frac{1}{Q} \left.\frac{\partial Q}{\partial \zeta}\right|_{N,V,T} = \frac{\int d\mathbf{r}^N \Phi_G(\mathbf{r}^N) \exp\{-[\Phi(\mathbf{r}^N) + \zeta\Phi_G(\mathbf{r}^N)]/kT\}}{\int d\mathbf{r}^N \exp\{-[\Phi(\mathbf{r}^N) + \zeta\Phi_G(\mathbf{r}^N)]/kT\}} = \langle \Phi_G \rangle_{N,V,T,\zeta}. \tag{A3}$$

Here, $\langle \Phi_G \rangle_{N,V,T,\zeta}$ denotes the canonical ensemble average of the ghost field potential $\Phi_G(\mathbf{r})$ for the fluid of loading N equilibrated in the ghost field of the magnitude ζ. $\langle \Phi_G \rangle_{N,V,T,\zeta}$

is calculated by weighting the ghost field potential along N_R isostere with the average fluid density $\rho_{N,\zeta}(\mathbf{r})$ in the ghost field of the magnitude ζ:

$$\langle \Phi_G \rangle_{N,V,T,\zeta} = \int_V \Phi_G(\mathbf{r}) \rho_{N,\zeta}(\mathbf{r}) d^3\mathbf{r}. \quad \text{(A4)}$$

The integration of Eq. (A3) leads to Eqs. (14) and (17), which determine the change of the Helmholtz free energy of the system in the process of turning on (off) the ghost field along N_0 and N_R isosteres.

[1] J. K. Lee, J. A. Barker, and F. F. Abraham, J. Chem. Phys. **58**, 3166 (1973).
[2] D. J. McGinty, J. Chem. Phys. **58**, 4733 (1973).
[3] A. I. Rusanov and E. N. Brodskaya, J. Colloid Interface Sci. **62**, 542 (1977).
[4] S. Ono and S. Kondo, in *Encyclopedia of Physics*, edited by S. Flugge (Springer, Berlin, 1960), Vol. 10.
[5] J. S. Rowlinson, Physica B & C **127**, 276 (1984).
[6] J. W. Gibbs, *The Scientific Papers of J. Willard Gibbs* (Dover, New York, 1961).
[7] R. C. Tolman, J. Chem. Phys. **17**, 333 (1949).
[8] S. Toxvaerd, J. Chem. Phys. **115**, 8913 (2001).
[9] H. Reiss and D. Reguera, J. Phys. Chem. B **108**, 6555 (2004).
[10] K. Binder, Physica A **319**, 99 (2003).
[11] D. Reguera, R. K. Bowles, Y. Djikaev, and H. Reiss, J. Chem. Phys. **118**, 340 (2003).
[12] A. Vishnyakov and A. V. Neimark, J. Phys. Chem. **109**, 5962 (2005).
[13] A. Harasima, Adv. Chem. Phys. **1**, 203 (1958).
[14] P. Schofield and J. R. Henderson, Proc. R. Soc. London **379**, 231 (1982).
[15] J. S. Rowlinson, Pure Appl. Chem. **65**, 873 (1993).
[16] S. M. Thompson, K. E. Gubbins, J. Walton, R. A. R. Chantry, and J. S. Rowlinson, J. Chem. Phys. **81**, 530 (1984).
[17] M. J. P. Nijmeijer, C. Bruin, A. B. Vanwoerkom, A. F. Bakker, and J. M. J. Vanleeuwen, J. Chem. Phys. **96**, 565 (1992).
[18] M. J. P. Nijmeijer, C. Bruin, and J. M. J. vanLeeuwen, J. Chem. Phys. **100**, 7844 (1994).
[19] M. J. Haye and C. Bruin, J. Chem. Phys. **100**, 556 (1994).
[20] M. Mareschal, M. Baus, and R. Lovett, J. Chem. Phys. **106**, 645 (1997).
[21] P. R. ten Wolde and D. Frenkel, J. Chem. Phys. **109**, 9901 (1998).
[22] H. El Bardouni, M. Mareschal, R. Lovett, and M. Baus, J. Chem. Phys. **113**, 9804 (2000).
[23] E. N. Brodskaya and A. I. Rusanov, J. Chem. Phys. **100**, 7844 (1994).
[24] E. N. Brodskaya, Colloid J. **63**, 15 (2001).
[25] T. Ikeshoji, B. Hafskjold, and H. Furuholt, Mol. Simul. **29**, 101 (2003).
[26] G. M. Torrie and J. P. Valleau, J. Comput. Phys. **23**, 187 (1977).
[27] D. Frenkel and B. Smit, *Understanding Molecular Simulation. From Algorithms to Applications* (AP, San Diego, 1996).
[28] I. Kusaka and D. W. Oxtoby, J. Chem. Phys. **110**, 5249 (1999).
[29] I. Kusaka, Z. G. Wang, and J. H. Seinfeld, J. Chem. Phys. **108**, 3416 (1998).
[30] B. Chen, J. I. Siepmann, K. J. Oh, and M. L. Klein, J. Chem. Phys. **115**, 10903 (2001).
[31] H. Reiss, A. Tabazadeh, and J. Talbot, J. Chem. Phys. **92**, 1266 (1990).
[32] J. Merikanto, H. Vehkamaki, and E. Zapadinsky, J. Chem. Phys. **121**, 914 (2004).
[33] F. H. Stillinger, J. Chem. Phys. **38**, 1486 (1963).
[34] A. Vishnyakov and A. V. Neimark, J. Chem. Phys. **119**, 9755 (2003).
[35] A. V. Neimark and A. Vishnyakov, Phys. Rev. E **62**, 4611 (2000).
[36] A. Vishnyakov and A. V. Neimark, J. Phys. Chem. B **105**, 7009 (2001).
[37] Y. Viisanen, R. Strey, and H. Reiss, J. Chem. Phys. **99**, 4680 (1993).
[38] D. Kashchiev, J. Chem. Phys. **76**, 5098 (1982).
[39] J. W. P. Schmelzer, J. Colloid Interface Sci. **242**, 354 (2001).
[40] J. K. Johnson, J. A. Zollweg, and K. E. Gubbins, Mol. Phys. **78**, 591 (1993).
[41] M. Mecke, J. Winkelmann, and J. Fischer, J. Chem. Phys. **107**, 9264 (1997).
[42] J. J. Potoff and A. Z. Panagiotopoulos, J. Chem. Phys. **112**, 6411 (2000).
[43] J. R. Errington, Phys. Rev. E **67**, 031107 (2003).
[44] C. D. Holcomb, P. Clancy, and J. A. Zollweg, Mol. Phys. **78**, 437 (1993).
[45] See EPAPS Document No. E-JCPSA6-122-510518 for four supplementary figures. Figure S1 is a collection of literature data on the planar surface tension of uncut LJ fluid. Figures S2–S4 show the density, energy, and pressure profiles of LJ clusters obtained in MD simulations. A direct link to this document may be found in the online article's HTML reference section. The document may also be reached via the EPAPS homepage (http://www.aip.org/pubservs/epaps.html) or from ftp.aip.org in the directory epaps/. See the EPAPS homepage for more information.
[46] G. E. Norman and V. S. Filinov, High Temp. **7**, 216 (1969).
[47] D. J. Adams, Mol. Phys. **29**, 307 (1975).
[48] H. Reiss, J. L. Katz, and E. R. Cohen, J. Chem. Phys. **48**, 5553 (1968).
[49] K. J. Oh and X. C. Zeng, J. Chem. Phys. **108**, 4683 (1998).
[50] R. McGraw and A. Laaksonen, Phys. Rev. Lett. **76**, 2754 (1996).
[51] R. McGraw and A. Laaksonen, J. Chem. Phys. **106**, 5284 (1997).
[52] P. I. Ravikovitch, A. Vishnyakov, R. Russo, and A. V. Neimark, Langmuir **16**, 2311 (2000).